Change of evaporation rate of single monocomponent droplet with temperature using time-resolved phase rainbow refractometry

Yingchun Wu[a,*], Haipeng Li[c], Xuecheng Wu[a], Gérard Gréhan[d], Lutz Mädler[c], Cyril Crua[b]

[a]State Key Laboratory of Clean Energy Utilization, Zhejiang University, Hangzhou, 310027, China
[b]Advanced Engineering Centre, University of Brighton, Brighton BN2 4GJ, UK
[c]Leibniz Institute for Materials Engineering IWT, Faculty of Production Engineering, University of Bremen, Bremen, 28359, Germany
[d]CNRS UMR 6614/CORIA, BP12, 76801 Saint Etienne du Rouvray, France

Abstract

Droplet evaporation characterization, although of great significance, is still challenging. The recently developed phase rainbow refractometry (PRR) is proposed as an approach to measuring the droplet temperature, size as well as evaporation rate simultaneously, and is applied to a single flowing n-heptane droplet produced by a droplet-on-demand generator. The changes of droplet temperature and evaporation rate after a transient spark heating are reflected in the time-resolved PRR image. Results show that droplet evaporation rate increases with temperature, from -1.28×10^{-8} m^2/s at atmospheric 293 K to a range of $[-1.5, -8] \times 10^{-8}$ m^2/s when heated to [294, 315] K, agreeing well with the Maxwell and Stefan-Fuchs model predictions. Uncertainty analysis suggests that the main source is the indeterminate gradient inside droplet, resulting in an underestimation of droplet temperature and evaporation rate. With the demonstration on simultaneous measurements of droplet refractive index as well as droplet transient and local evaporation rate in this work, PRR is a promising tool to investigate single droplet evaporation in real engine conditions.

Keywords:
Phase rainbow refractometry, droplet, size change, temperature, evaporation rate

*Corresponding author: wycgsp@zju.edu.cn

1. Introduction

Droplet heating and evaporation are coupled heat and mass transfer processes accompanying droplet combustion, which is widely applied in liquid fuel powered devices, such as gas turbines and internal combustion engines, etc. The droplet temperature increases upon its ejection into a hot gas medium until its surface temperature approaches boiling temperature, and meanwhile the droplet evaporation rate also changes dramatically because of its strong dependence on droplet temperature. The evaporation rate influences droplet life-time, local mixing and air-fuel ratio and eventually combustion [1–5], and vice versa [6]. Thus droplet temperature and evaporation rate are key parameters in both experimental and numerical investigations on droplets and sprays combustion [7–9]. Droplet evaporation behaviors have attracted intensive investigations [10–12], from mono-component [13, 14] to multicomponent [15–19] at standard conditions as well as elevated temperature and pressure conditions [20–29].

A quantitative and simultaneous measurement of flowing droplet temperature and evaporation rate is of great importance, but involves multiple trans-scale parameters and thus is challenging, especially for droplets with size below 100 μm. For the droplet temperature determination, spectroscopic imaging is widely employed, and techniques of this category include laser-induced fluorescence (LIF) [26, 30–32], and laser induced phosphorescence (LIP) [33]. The Lagrangian strategy by tracking droplet images via various visualization techniques is commonly applied to investigate the average evaporations of suspended [17, 19, 21, 24, 25, 27, 28], levitated [15] or flowing droplets [23, 34, 35]. An alternative to droplet imaging is morphology dependent resonance (MDR) [15, 35], that monitors droplet size with accuracy up to hundreds of nanometer, with the limit of perfectly spherical droplet. Recently, phase interferometric particle imaging (PHIPI) was developed to measure very small changes in droplet size via the time-resolved light scattering fringes at forward direction [36]. Rainbow refractometry can precisely measure droplet temperature/refractive index via rainbow position [8, 15, 37, 38]. Its recent advances from traditional point-probe standard/global rainbow techniques to one-dimensional phase rainbow refractometry (PRR) [39–41], permits accurate measurement of droplet size changes, in addition to droplet temperature and size. This capability makes PRR an ideal tool for transient droplet evaporation/condensation characterization, in which processes droplet size undergoes tiny changes in the order of micrometer or even less. In [39, 41], the PRR was applied to droplet streams with a low sampling frequency (less than twenty Hz), but impractical to monitor the evaporation rate of a single droplet.

Most of measurements of droplet evaporation rate were conducted under a constant droplet temperature. While in real spray combustion applications, droplets are heated up with the evaporation rate increasing. In some extreme cases, droplets are subject to a transient heat, i.e., spark heating in spark ignition (SI) engines or flame heating when passing through a flame front, while evaporation rates of those processes have been rarely measured experimentally, due to the lack of proper tools. Technically, by using a single lens and a high speed linear camera rather than an imaging system with three lenses, two slits and a planar sensor as in previous PRR systems [39, 41], this work introduces a simple and low-cost implementation of a time resolved PRR with sampling frequency up to 67 kHz. Based on this technique, the change of droplet temperature and transient evaporation rate of a single isolated droplet under a transient heat are experimentally determined, demonstrating an approach for experimental investigation of the aforementioned problems. Below is details of the time resolved PRR technique, experimental configuration and results.

2. Methodology

2.1. Phase rainbow refractometry (PRR)

As schematically shown in Fig. 1a, rainbow light of a droplet with refractive index (n) mainly contains two orders of its light scattering according to van de Hulst's notation [42]. The dominant one is the second order refraction experiencing one internal reflection at droplet inner surface, denoted by $p=2$ in Debye series, and generates Airy rainbow. The rainbow angle locates at the minimum inflection angle, and the angular position (θ_{rg}) of the corresponding ray, which is called Descartes ray according to geometric optics, can be derived as follows.

$$\theta_{rg} = 4\arccos\left(\frac{1}{n}\sqrt{\frac{4-n^2}{3}}\right) - 2\arcsin\left(\sqrt{\frac{n^2-1}{3}}\right) \quad (1)$$

The other light is the reflection at droplet outer surface, denoted by $p=0$ in Debye series. It is much weaker than the refraction ($p=2$), and thus their interference produces high frequency ripples superimposed on Airy rainbow. The droplet refractive index and size can be simultaneously retrieved from the rainbow angle position (according to Eq. 1) and light distribution of its
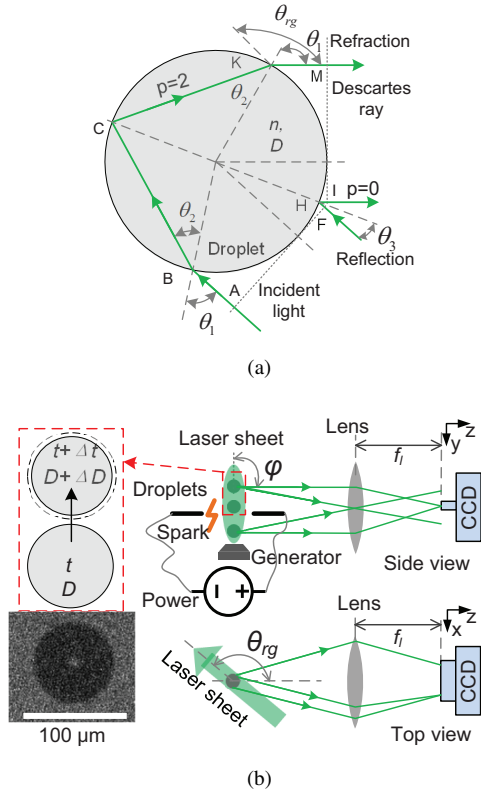
(a)

100 μm

(b)

Fig. 1: Schematics of rainbow formation and experimental configuration of PRR for single droplet measurements. (a) Trajectories of the refraction and reflection light in rainbow of a droplet. (b) Experimental setup for measurement of flowing and evaporating droplet with time resolved PRR.

transient rainbow signal in standard rainbow refractometry (SRR). However, the size change ΔD can not be accurately obtained in a Lagrangian approach that directly compares the measured size D via SRR at different times. This is because the size change during the short time interval due to evaporation is at nanometer scale, which is one order less than the accuracy in size measurement with SRR. For an evaporating droplet, as illustrated by the inset in Fig. 1b, the tiny size change causes small variations to optical path lengths of the refraction and reflection which are respectively $L_{p2} = L_{AB}+L_{BC}+L_{CK}+L_{KM}$ and $L_{p0} = L_{FH}+L_{HI}$, as well as to their optical path length difference, $L_d = L_{p0} - L_{p2}$, which eventually leads to a phase shift of their interference fringes, resulting in ripple structures. The relationship between size change of a homogeneous sphere and the phase shift ($\Delta\phi_{d,rg}$) of ripple fringes has been revealed [41],

$$\Delta D = c_{rg}\Delta\phi_{d,rg} \qquad (2)$$

The coefficient (c_{rg}) at the Airy rainbow angle is,

$$c_{rg} = \frac{\lambda}{2\pi} \frac{3^{3/2}n^2}{(8 + 10n^2)\sqrt{n^2 - 1}} \qquad (3)$$

where λ is the light wavelength.

With the obtained droplet size D and size change ΔD over time interval Δt, the transient evaporation rate can be measured directly as follows.

$$k_e = \frac{\left[(D + \Delta D)^2 - D^2\right]}{\Delta t} = \frac{2D\Delta D}{\Delta t} + o\left(\frac{\Delta D^2}{\Delta t}\right) \qquad (4)$$

2.2. Experimental setup

Figure 1b schematically shows the setup for the measurement of a single evaporating droplet. Single droplets of n-heptane were reproducibly generated with a droplet-on-demand generator at a frequency of 4 Hz, ejected into free space with an ambient temperature of 295.9 K, and moved vertically upward. The initial droplet diameter (D) was measured using a microscopic shadowgraph imaging with a value of 81-82.5 μm, as the droplet image shown in the inset of Fig. 1b. The droplet velocity was measured using a high-speed camera. An oxygen co-flow was delivered to the plastic square frustum with a length of 10 mm, and flowed along with the generated droplets, with the velocity controlled by a mass flow controller. In order to produce a uniform flow around the droplets, the dimension of the co-flow was about 120 times that of the droplets. The relative velocity (u) between the droplet and co-flow was in the range of 0.5 m/s to 2 m/s.

3

The evaporating single droplet was measured with a PRR system. A 3 Watts high power continuous laser sheet, with a wavelength (λ) of 532 nm and a height and width of 20 mm and 2 mm, respectively, illuminated the moving droplets. The laser beam was vertically polarized and thus the rainbow was contained in the perpendicular light scattering in the horizontal plane. The scattered light from the droplet around the primary rainbow angle was collected with a spherical lens (focal length 6.56 mm). The rainbow signal was recorded by a high-speed linear CCD camera. The line sensor of the camera, which has 1024×1 pixels, was placed in the horizontal (x-z) plane at the focal plane of the lens, and thus the camera only captured the rainbow light that is parallel to the x-z plane, i.e., φ=90°, as illustrated by Fig. 1b. This Fourier imaging system eliminates angular shift of rainbow signal along with the azimuth (φ) angle and droplet transversal displacement, ensuring an accurate recording. The camera was operated at a frequency of 67 kHz to record the rainbow light scattering of the moving and evaporating single droplets, forming a time-resolved PRR image. During the recording, an electrical spark was discharged to heat the droplet. The energy of the spark was adjusted to avoid igniting the droplet. Thus, rainbow signals of droplet before and after a transient heating by the spark were recorded in the same PRR image, and this neutralizes all other effects on these two processes and enables investigating the change of droplet evaporation rate with temperature. Each PRR image was synthesized from 1024 samples with 1024×1024 pixels. More details can be found in [38].
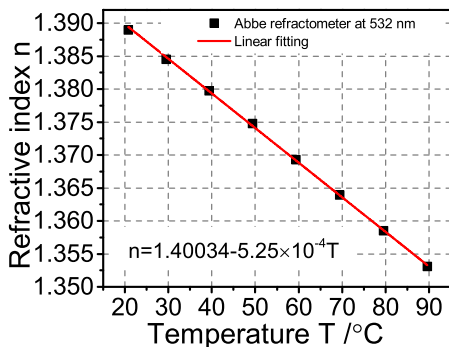

Fig. 2: Calibrated relationship between refractive index and temperature of n-heptane at 532 nm.

In order to quantitatively retrieve droplet refractive index from the recorded rainbow signal, the absolute scattering angle of the image pixel recorded by the camera was calibrated, and the angular resolution in the hor-izontal direction of each pixel is 0.01°. The refractive indices of n-heptane in the temperatures from 293 K to 363 K were measured with an Abbe refractometer. Then interpolation was performed to obtain the relationship between the refractive index and temperature of n-heptane droplet at 532 nm, as shown in Fig. 2. This relationship is used to quantitatively evaluate droplet temperature from its measured refractive index. Calibration shows that the refractive index of n-heptane at 532 nm reduces 0.000522 per degree.

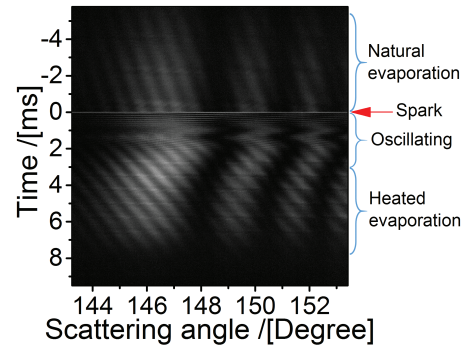## 3. Results and discussions

3.1. Experimental results

Fig. 3: A representative experimental PRR image of n-heptane droplets with a spark heating.

Figure 3 shows a representative experimental PRR image of a n-heptane droplet before and after a spark heating, which depicts the evolution of rainbow. The moment of spark heating is indicated by the white line, and regarded as the zero time. Tilted ripple fringes are observed before and after the electrical spark heating, and indicate the droplet was evaporating. The rainbow in Fig. 3 starts to change dramatically upon the spark heating, which induces a strong disturbance to the flow field and subsequently to a hydrodynamic instability to the droplet. The droplet is deformed due to the momentum transfer from the spark and flow, and oscillates as a result of surface tension. Consequently, the rainbow signal is completely distorted, as shown by the oscillation region in Fig. 3, because rainbow is highly sensitive to droplet morphology and rainbow of an ellipsoid could have complicated patterns, i.e., caustics [43]. Thus, this oscillating and nonspherical period is not studied in this work. The oscillation amplitude decays with the time due to the viscosity, and thus the droplet restores its spherical shape rapidly in about 2.5-3 ms after the spark, as evidenced by the reappearance of the typical standard

rainbow signal. Meanwhile, the droplet is heated by the spark via convection and radiation. From the calibration in Fig. 2, the droplet refractive index decreases with the temperature, and so does the rainbow angular position, as shown in Fig. 3. It is also observed that the tilt angle of the ripple fringes is larger after the spark compared to times [-4 ms, 0 ms]. As revealed by previous findings [39, 41], the inclining degree of the rainbow ripple, which corresponds to the phase shift of the ripples, relates to the size change and therefore the evaporation rate of the droplet. Thus, the phenomenon which has a decrement in the rainbow angular position associated with an increment in ripple fringes inclination in Fig. 3, is actually a direct observation of the change of droplet evaporation rate with temperature after heated by a spark.
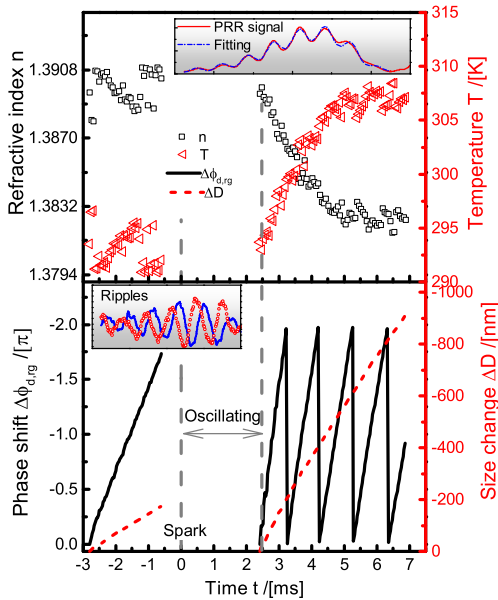

Fig. 4: PRR for droplet temperature and size change measurement. Upper: refractive index and temperature evolution of droplet in Fig. 3 after spark heating. Lower: the phase shift angle in PRR and the linked size change of the evaporating droplet.

Both the droplet temperatures and evaporation rates during time regions of [-2.5 ms, -0.5 ms] before heating and [2.5 ms, 7 ms] after spark are quantitatively evaluated, as demonstrated by the upper and lower parts of Fig. 4, respectively. Both regions are divided as a set of individual rainbow signals, with each averaged within about 60 μs and a time step between two adjacent signals of 30 μs. The refractive index and diameter are yielded by automatically searching the closest fitting to the experimental rainbow signal among the candidate rainbow signals calculated from the modified complicated angu-

lar momentum theory [44], and the upper inset of Fig. 4 demonstrates an accurate rainbow signal inversion signified by the global alignment in Airy rainbow position as well as the local match in fine ripples. Note that there is a rather sudden jump in refractive index and an associated decrease in temperature before the spark. This is mainly caused by the collaborative influences of periodical ripples and morphology-dependent resonances on the optimal fitting algorithm, which could terminate at a local optimization rather than a global one, leading to jumps. Results of sixty droplets show that their initial temperatures are stabilized around 293.2±0.8 K, which is a little lower than the room temperature due to heat loss caused by natural evaporation. While the droplet temperatures after a spark heating vary substantially, with the mean temperature from 294 K to 315 K. As exemplified by the results of Fig. 3 in Fig. 4, the droplet temperature increases from about 295 K to about 305 K during [2.5 ms, 5 ms] by the spark, and after about 5 ms the temperature is stable. The differences in droplet mean temperature and heating rate can be attributed to the different heating processes, i.e., different relative position between the spark arc and droplet.

With the determined droplet refractive index and diameter, then the droplet size change and subsequently evaporation rate are measured using the method proposed in [41]. Here we briefly recall the algorithm. The Airy rainbow of the droplet is computed using the measured droplet mean refractive index and diameter, and then it is subtracted from the experimental rainbow signal, yielding the separated ripple fringes, as a pair of ripples shown in the lower inset of Fig. 4. The droplet size change ΔD during a time interval Δt is obtained according to Eq. 2 by evaluating the phase shift $\Delta \phi_{d,rg}$ between their ripple fringe pair from their cross power spectrum density (CPSD). The size changes and thereafter evaporation rates of both regions before and after the spark heating are calculated, as shown in the lower panel of Fig. 4. Results show that size changes and evaporation rates are quite stable before the spark heating, with an evaporation rate of -1.28±0.04×10^{-8} m^2/s, confirming with the former measurement [41]. The stabilities in the measured refractive indices and evaporation rates before the spark heating imply the identities of the generated droplets, the surrounding environments and their interactions during that region. While similar to the droplet temperature, the droplet evaporation rate after the spark heating also varies in a quite large range between -1.5 ×10^{-8} m^2/s and -8 ×10^{-8} m^2/s.

3.2. Evaporation model comparison

The theoretical evaporation rates of a moving droplet at the experimental conditions were also computed using the Maxwell and Stefan-Fuchs model according to the following equation [11, 45],

$$k_t = 4D_v \frac{\rho_g}{\rho_l} \text{Sh} \ln\left(1 + B_M\right) \qquad (5)$$

where D_v is the diffusion coefficient of the vapor, and ρ_g and ρ_l are the densities of the gas surrounding the droplet, and of the droplet's liquid phase, respectively. The Sherwood number (Sh) is calculated with the correlation [46],

$$\text{Sh} = 2.009 + 0.514\text{Re}^{1/2}\text{Sc}^{1/3} \qquad (6)$$

where $\text{Re} = uD/\nu$ is the Reynolds number, with u the velocity of the gas with respect to the droplet and ν the kinematic viscosity of the vapor. $\text{Sc} = \nu/D_v$ is the Schmidt number. $B_M = (\rho_{vs} - \rho_{v\infty})/\rho_{gs}$ is the Spalding mass transfer number, where ρ_{vs}, $\rho_{v\infty}$ are the mass density of the vapor at the droplet surface and at infinity for the saturated pressured relating to the droplet temperature, respectively, and ρ_{gs} is the gas density surrounding the droplet. Note that ρ_{vs} is controlled by the droplet surface temperature, and is approximated as the temperature measured with rainbow refractometry in this work. $\rho_{v\infty}$ is assumed to be zero in the calculation. The theoretical evaporation rates of n-heptane droplets at measured mean temperatures are calculated using temperature-dependent properties obtained from NIST [47].
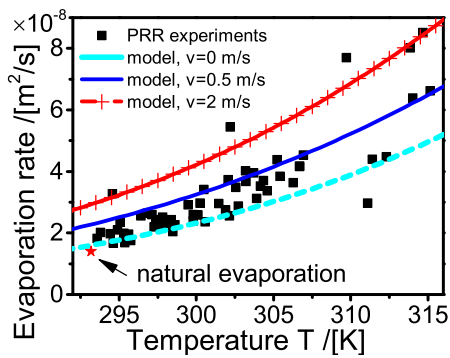

Fig. 5: Measured evaporation rates of sixty n-heptane droplets at different temperatures and their comparisons with model predictions.

Figure 5 shows the experimental droplet evaporation rate versus droplet temperature measured with PRR, and the star denotes the natural evaporation rate before spark heating. It is found that the droplet evaporation rate obviously increases with temperature in the experimental region. The theoretical evaporation rates of a moving droplet at the experimental conditions were also plotted in Fig. 5 for comparison. The lower and upper boundaries of the band correspond to velocities of 0.0 m/s and 2 m/s, respectively. At zero relative velocity, where the Re number reduces to 0 and Sherwood number (Sh) approaches 2, the vapor diffuses away from the droplet which determines the evaporation rate. The theoretical evaporation rate before the spark heating is -1.36×10^{-8} m^2/s, consistent with but still a little larger than the experimental value, which could be partially explained that the droplet surface temperature is a little lower than the droplet average temperature in natural evaporation. This means that the droplet almost fully follows the co-flow, and also demonstrates the feasibility and accuracy of droplet evaporation rate measured with PRR. While after the spark heating, the droplet evaporates faster than those at zero velocity conditions, and close to theoretical values with velocities between 0.5 m/s to 2 m/s. This is because the gas gains a relative velocity when it is heated by the spark resulted from thermal buoyancy. The vapor is transferred away by the convection in additional to the diffusion, which also increases with the temperature. Thus, the droplet evaporation rate increases as a result of these two collaborative effects. A comparison between the experimental and theoretical values shows that they agree well with each other in the general qualitative trend as well as quantitative values.

3.3. Uncertainty analysis

Despite the good quality of the experimental PRR images and the accurate inversion algorithm, the measurements of refractive index (temperature) and evaporation rates have some uncertainties. This includes the systematic uncertainty that arises from the optical measurement system and from the inversion algorithm. Errors in absolute scattering angle calibration of the captured rainbow signal, which might be caused by the limited resolution of the rotation platform and pixel pitch is up to 0.05°. This leads to uncertainties of $\pm 3 \times 10^{-4}$ and 0.6°C in droplet refractive index and temperature, respectively. Another source of uncertainty is from the inversion algorithm. Since ripple structures are taken into account during the optimization, the target function is not monotonic but is superimposed with ripples which are ascribed to the periodical variation of ripple with the size parameter. Besides, the semi-classical complex angular momentum theory for the fast calculation of rainbow is an asymptotic approximation of the exact Debye series (p=0, 2). Subsequently, the search for an optimal

match between the measured and simulated rainbows could terminate at a local optimization near the global optimum. Hence the accuracy of the refractive index measurement is in the fourth digit with an uncertainty of about $\pm 4\times 10^{-4}$. Thus, the systematic temperature uncertainty is about ± 1.4 °C in total.

Another important issue for the uncertainty is the inhomogeneity of the real droplets. As the droplet subject to heating and evaporation, a negative temperature gradient and a positive refractive index gradient are developed from the droplet surface to the inner core. Provided that the isolated droplet is radially symmetrical with one-dimensional gradient at the experimental low Reynolds number (Re) region, the light refracted into the droplet bends and its trajectory is a curve inside the gradient droplet. The primary rainbow position of an inhomogeneous droplet depends on both the absolute value and its profile. The difference between the homogeneous model and physically inhomogeneous process brings about an inevitable indeterminacy in refractive index measurement and the linked droplet temperature as well, even though it is always possible to find a good fitting in both rainbow position and even ripple structure in the inversion. The obtained refractive index/temperature is neither the droplet surface refractive index/temperature nor the droplet core refractive index/temperature. It is also worth mentioning that the droplet reaches a virtually homogeneous refractive index/temperature distribution in a short fraction of the characteristic time, and thus the influence of heating is restricted to a short period after the transient heating, which is mainly the oscillating period [48]. The measured refractive index/temperature is a kind of average value close to the outer region, and the region in which the rainbow light trajectory locates is usually less than half of the droplet radius [48]. Previous analysis of heated heptane droplets revealed that the uncertainty of refractive index measurement can be up to 5% - 10% [37].

According to Eq. 4, the uncertainty of droplet evaporation rate arises from indeterminacies in droplet diameter and its regressing rate. The droplet size, determined in PRR has an accuracy of $\pm$ 1.5 µm and a relative uncertainty of about 2%. Concerning the size change rate measurement according to Eq. 2, the phase shift angle and the coefficient, whose accuracy can be affected by the above refractive index and size uncertainty, are the two main sources. Errors of droplet refractive index and size measurement have little influences in the phase shift measurement because it is a relative and averaged one with respect to the reference ripple fringe. Thus, the measured phase shift has a discrepancy as low as 0.6% in this work. The uncertainty of the coefficien-

t plays a determinant role in evaporation rate accuracy, and lies in two parts. One uncertainty calculated from Eq. 3 is induced by the measured refractive index error, but with value less than 1%. Note that Eq. 2 is derived on the hypothesis of homogeneous sphere, which would not strictly hold and is an approximation of the heated and evaporating droplet in the experiment. The exact bent trajectory of the light inside the droplet is difficult to ascertain because of the unknown of the exact gradient profile, and thus it is difficult to quantify its effects on the size change measurement. The responses of the phase of interferometric ripples can be evaluated by modeling the radially symmetric droplet with a continuous internal refractive index profile using geometric optics [49] or a multilayered sphere by rigorous light scattering [50]. The gradient of a heated droplet shifts the ripple fringes opposite to the direction by droplet size reduction and partially counterbalances the phase shift angle. This suggests that the coefficient calculated by Eq. 3 is underestimated. If the gradient is steady and the droplet approaches a so-called 'wet-bulb' equilibrium (page 109 of [45]), where the heat transferred to the droplet is all spent on evaporation, the curved light trajectory keeps unchanged and underestimation of size change is minimized at this condition. While at other conditions, the heat penetrates droplet surface and transfers inside, causing changes of temperature and refractive index profiles and subsequently light trajectory. Then, this worsens the accuracy with discrepancy up to 10% or even higher. From the above analysis, the measured droplet temperatures were lower than droplet surface temperatures, and the evaluated evaporation rates are less than their real values, and the amount of uncertainty mainly relies on the inhomogeneity of the gradients.

4. Conclusions

A time resolved one-dimensional phase rainbow refractometry, with simple configuration and robust performance, has been applied to measure droplet refractive index/temperature, size and size changes, providing an ideal approach to droplet evaporation characterization. The evolutions of temperature and evaporation rate of single isolated droplet after a transient spark heating are investigated with the PRR system. The droplet temperature measured by PRR tends to reflect the region close to droplet surface. Experimental measurements show that droplet evaporation rate obviously increases with temperature after spark heating, and are well consistent with predictions by evaporation model. The measurement uncertainty is mainly attributed to the droplet

inhomogeneity, and both temperature and evaporation rate are underestimated.

This work demonstrates that PRR permits the simultaneous measurement of droplet refractive index as well as droplet transient and local evaporation rate. Although only h-heptane droplet under ambient pressure was studied in this work, the PRR technique and the experimental apparatus can be extended to systematic studies of evaporations of different drops under varying conditions, e.g., multiple component droplets under engine-like conditions.

Acknowledgments

[1] J. Xia, K.H. Luo, *Proc. Combust. Inst.* 33 (2011) 2581-2590.
[2] J.B. Greenberg, *Combust. Flame* 148 (2007) 187-197.
[3] C.G. Wang, A.M. Dean, H.Y. Zhu, R.J. Kee, *Combust. Flame* 160 (2013) 265-275.
[4] S. De, S.H. Kim, *Combust. Flame* 160 (2013) 2048-2066.
[5] W. Han, Z. Chen, *Combust. Flame* 162 (2015) 2128-2139.
[6] T. Kitano, J. Nishio, R. Kurose, S. Komori, *Combust. Flame* 161 (2014) 551-564.
[7] H.H. Chiu, *Prog. Energy Combust. Sci.* 26 (2000) 381-416.
[8] C. Letty, B. Renou, J. Reveillon, S. Saengkaew, G. Gréhan, *Combust. Flame* 160 (2013) 1803-1811.
[9] M.R.G. Zoby, S. Navarro-Martinez, A. Kronenburg, A.J. Marquis, *Proc. Combust. Inst.* 33 (2011) 2117-2125.
[10] M. Birouk, I. Gokalp, *Prog. Energy Combust. Sci.* 32 (2006) 408-423.
[11] S.S. Sazhin, *Prog. Energy Combust. Sci.* 32 (2006) 162-214.
[12] S.S. Sazhin, *Fuel* 196 (2017) 69-101.
[13] C.G. Yin, *Appl. Therm. Eng.* 104 (2016) 497-503.
[14] C. Verwey, M. Birouk, *Combust. Flame* 182 (2017) 288-297.
[15] J. Wilms, Evaporation of multicomponent droplets, Universität Stuttgart, Stuttgart, Germany, 2005.
[16] T. Kitano, J. Nishio, R. Kurose, S. Komori, *Fuel* 136 (2014) 219-225.
[17] H. Ghassemi, S.W. Baek, Q.S. Khan, *Combust. Sci. Technol.* 178 (2006) 1031-1053.
[18] L.M. Itani, G. Bruneaux, A. Di Lella, C. Schulz, *Proc. Combust. Inst.* 35 (2015) 2915-2922.
[19] X.K. Ma, F.J. Zhang, K. Han, B. Yang, G.Q. Song, *Fuel* 160 (2015) 43-49.
[20] H. Kim, N. Sung, *Combust. Flame* 135 (2003) 261-270.
[21] H. Ghassemi, S.W. Baek, Q.S. Khan, *Combust. Sci. Technol.* 178 (2006) 1669-1684.
[22] H.T. Zhang, V. Raghavan, G. Gogos, *Int. J. Spray Combust.* 1 (2009) 317-338.
[23] S. Horender, M. Sommerfeld, *Int. J. Spray Combust.* 4 (2012) 123-153.
[24] I. Javed, S.W. Baek, K. Waheed, G. Ali, S.O. Cho, *Combust. Flame* 160 (2013) 2955-2963.
[25] I. Javed, S.W. Baek, K. Waheed, *Combust. Flame* 160 (2013) 170-183.
[26] F. Lemoine, G. Castanet, *Exp. Fluids* 54 (2013) 1-34.
[27] M. Birouk, S.C. Fabbro, *Proc. Combust. Inst.* 34 (2013) 1577-1584.
[28] M. Birouk, *Combust. Sci. Technol.* 186 (2014) 1295-1308.
[29] C. Verwey, M. Birouk, *Combust. Flame* 189 (2018) 33-45.
[30] P. Lavieille, F. Lemoine, M. Lebouché, *Combust. Sci. Technol.* 174 (2002) 117-142.
[31] L. Perrin, G. Castanet, F. Lemoine, *Exp. Fluids* 56 (2015) 29.
[32] G. Castanet, L. Perrin, O. Caballina, F. Lemoine, *Int. J. Heat Mass Transf.* 93 (2016) 788-802.
[33] A. Omrane, G. Juhlin, F. Ossler, M. Aldén, *Appl. Opt.* 43 (2004) 3523-3529.
[34] D. Nguyen, D. Honnery, J. Soria, *Exp. Fluids* 50 (2011) 949-959.
[35] G. Chen, M.M. Mazumder, R.K. Chang, J.C. Swindal, W.P. Acker, *Prog. Energy Combust. Sci.* 22 (1996) 163-188.
[36] Y. Wu, H. Li, M. Brunel, J. Chen, G. Gréhan, L. Mädler, *Appl. Phys. Lett.* 111 (2017) 041905.
[37] P. Massoli, *Appl. Opt.* 37 (1998) 3227-3235.
[38] H. Li, C.D. Rosebrock, T. Wriedt, L. Mädler, *J. Quant. Spectrosc. Radiat. Transf.* 195 (2017) 164-175.
[39] J. Promvongsa, P. Vallikul, B. Fungtammasan, A. Garo, G. Gréhan, S. Saengkaew, *Proc. Combust. Inst.* 36 (2017) 2401-2408.
[40] X. Wu, H. Jiang, Y. Wu, J. Song, G. Gréhan, S. Saengkaew, L. Chen, X. Gao, K. Cen, *Opt. Lett.* 39 (2014) 638-641.
[41] Y. Wu, J. Promvongsa, S. Saengkaew, X. Wu, J. Chen, G. Gréhan, *Opt. Lett.* 41 (2016) 4672-4675.
[42] H.C. Hulst, H. Van De Hulst, Light scattering by small particles, Courier Corporation, USA, 1957.
[43] H. Yu, F. Xu, C. Tropea, *Opt. express* 21 (2013) 25761-25771.
[44] H. Nussenzveig, *J. Math. Phys.* 10 (1969) 125.
[45] S. Sazhin, Droplets and sprays, Springer, Berlin, Germany, 2014, p. 109.
[46] M. Kulmala, T. Vesala, J. Schwarz, J. Smolik, *Int. J. Heat Mass Transf.*, 38 (1995) 1705-1708.
[47] E.W. Lemmon, M.O. McLinden and D.G. Friend, available at: <http://webbook.nist.gov/cgi/cbook.cgi?ID=142-82-5>.
[48] K. Anders, N. Roth, A. Frohn, Particle & Particle Systems Characterization, 13 (1996) 125-129.
[49] M. Schneider, E.D. Hirleman, *Appl. Opt.*, 33 (1994) 2379-2388.
[50] R. Li, X.e. Han, H. Jiang, K.F. Ren, *Appl. Opt.*, 45 (2006) 1260-1270.